Geophysical Research Letters®

Key Points:

- The magnetopause is often observed several R_E upstream its nominal position under nearly radial IMF
- Extreme magnetopause displacements are accompanied with strong antisunward magnetosheath jets
- Reversal of the jet direction is **associated with** the magnetopause outward displacement

Correspondence to:

Z. Němeček,
zdenek.nemecek@mff.cuni.cz

Extremely Distant Magnetopause Locations Caused by Magnetosheath Jets

Z. Němeček[1] [iD]**, J. Šafránková[1]** [iD]**, K. Grygorov[1]** [iD]**, A. Mokrý[1], G. Pi[1]** [iD]**, M. Aghabozorgi Nafchi[1]** [iD]**, F. Němec[1]** [iD]**, N. Xirogiannopoulou[1]** [iD]**, and J. Šimůnek[2]**

[1]Faculty of Mathematics and Physics, Charles University, Prague, Czech Republic, [2]Institute of Atmospheric Physics, The Czech Academy of Sciences, Prague, Czech Republic

Abstract Magnetopause position is controlled mainly by the solar wind dynamic pressure and north-south interplanetary magnetic field component and these quantities are included in different empirical magnetopause models. We have collected about 50,000 of dayside magnetopause crossings observed by THEMIS in course of 2007–2019 and **compared** the observed magnetopause position with model prediction. The difference between observed and predicted magnetopause radial distance, $R_{obs} - R_{mod}$ is used for **quantifying** the model-observation agreement. Its median values are well predicted **for cases up to** $R_{obs} \approx 12\ R_E$ for all models but higher positive deviations are found for larger magnetopause distances, mainly under a nearly radial field and low dynamic pressure. The analysis reveals their connection with transient magnetopause displacements caused by strong sunward flows in the magnetosheath. We discuss **the possible** origin of the observed magnetosheath flow switching in terms of the interaction of magnetosheath jets with the magnetopause.

Plain Language Summary Comparison of the observed magnetopause crossings with prediction of the magnetopause models reveals that under nearly radial interplanetary magnetic field can be the magnetopause observed several Earth radii farther from the Earth than the models predict. Comprehensive examination of several cases characterized by suitable spacecraft locations leads to the conclusion that the source of such magnetopause displacements is connected with the reformation of nearly parallel bow shock resulting in a strong antisunward jet in the magnetosheath. The jet creates a dip in the magnetopause surface that reverses its direction. The sunward flow in the magnetosheath pulls the magnetopause also sunward. Since these effects are transient in their nature, they cannot be captured by statistical magnetopause models.

1. Introduction

The magnetopause (MP) is a critical boundary dividing the space controlled by the Earth magnetic field from the solar wind and interplanetary magnetic field (IMF). Its position is influenced mainly by the solar wind dynamic pressure and the north-south IMF component (B_Z) and these quantities are included in a variety of empirical MP models. To give several examples: the Jelínek et al. (2012) model uses a paraboloid of revolution oriented along the solar wind velocity and scaled with the dynamic pressure as $P_d^{-1/5.2}$ but does not apply IMF B_Z or other parameters; Petrinec and Russell (1996) use different functional forms for the dayside and nightside magnetopauses, both are ellipsoids of revolution scaled with IMF B_Z and the dynamic pressure scaling exponent is $P_d^{-1/6}$; probably the most popular Shue et al. (1997) model is based on an ellipsoid of revolution oriented along the solar wind velocity scaled with the dynamic pressure as $P_d^{-1/6.6}$, IMF B_Z changes MP dimensions as well as the flaring angle; a newer model by Lin et al. (2010) uses a similar functional form as Shue et al. (1997) scaled with the sum of magnetic and dynamic pressures as $P_d^{-1/5.15}$ and applies corrections for the MP indentation in the cusp region (Boardsen et al., 2000; Šafránková et al., 2005; Suvorova et al., 2005). In course of time, different authors used various approaches and methods for development of new MP models that include other scaling parameters (e.g., Liu et al., 2015; Nguyen et al., 2022; Wang et al., 2013; Xu et al., 2022 and more) or studied an influence of different parameters on the MP location (Dušík et al., 2010; Gu et al., 2023; Machková et al., 2019; Samsonov et al., 2019; Staples et al., 2020). The performance of several older MP models was tested by Šafránková et al. (2002) using about 3500 MP crossings and the authors have shown that the differences between their predictions are small in a statistical sense even though the prediction errors can reach more than 1 R_E (Earth's radius) in individual cases.
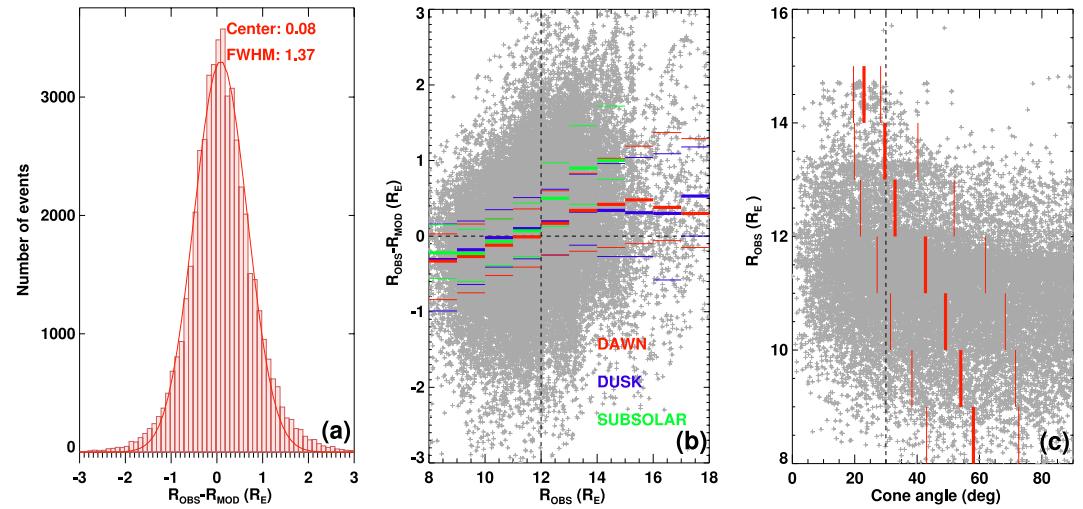
Figure 1. (a) Distributions of $R_{obs} - R_{mod}$; (b) $R_{obs} - R_{mod}$ as a function of R_{obs}; and (c) R_{obs} as a function of the cone angle; all for subsolar crossings. The Lin et al. (2010) model and OMNI database are used for R_{mod}. The heavy broken lines in panels (b) and (c) show medians in distance bins and the thin lines stand for the first and third quartiles.

A statistical study of extreme magnetopause locations (Grimmich et al., 2023) reveals that the high upstream Mach number, enlarged plasma β and low IMF cone angle (the angle between the IMF vector and X_{GSE} axis) are often connected with a large magnetopause expansion. However, these parameters are not independent because prolonged intervals of a low IMF cone angle are usually connected with depressed magnetic field magnitude (Pi et al., 2014) that implies the enhanced β and Mach number and thus it is not clear which of these parameters is more important in the magnetopause location setting.

The large deviation from the model can be also connected either with a wrong prediction of upstream conditions, especially with timing of arrivals of the interplanetary shocks and other discontinuities, or with transient phenomena like hot flow anomalies (HFAs) (Jacobsen et al., 2009; Šafránková et al., 2012; Sibeck et al., 1999) that result from the interaction of IMF tangential discontinuities with bow shock (BS). Such interaction is characterized by a creation of the region of the depleted pressure in BS front leading to quick outward motions of both BS and MP. The outward BS motion can be complemented with the sunward flow in the magnetosheath (Archer et al., 2014). Plaschke et al. (2017) explain the magnetosheath sunward flow by the interaction of an intense earthward propagating magnetosheath jet with the ambient magnetosheath plasma. The magnetosheath sunward flow following the arrival of a weak IMF directional discontinuity was also reported by Shue et al. (2009). The authors suggest that the interaction leads to formation of an antisunward jet creating a dip on the MP surface that reverses the jet direction.

A comparison of observed MP locations with model predictions can serve as a proof of our understanding of the interaction between the solar wind and Earth magnetic field. Since corresponding upstream conditions are usually derived from observations at the L1 point, our knowledge on solar wind propagation and evolution on short scales are tested as well. In order to improve our understanding of the processes involved in the MP formation, the present study is devoted to the analysis of sources of large positive deviations of the MP location from the predicted positions and to the search for the conditions under which they arise.

2. Data Set and Motivation

We have collected more than 50,000 dayside MP crossings observed in course of the 2007–2021 years by the THEMIS spacecraft fleet (Angelopoulos, 2008). These crossings were identified by the routine based on the Jelínek et al. (2012) region identification method and partly **verified** by visual inspection of plots of magnetic field (Auster et al., 2008) and plasma (McFadden et al., 2008) parameters. For each of the crossings we computed the model MP position using four models (Jelínek et al., 2012; Lin et al., 2010; Petrinec & Russell, 1996; Shue et al., 1997) and the OMNI solar wind data as their input. An example of the observation–model comparison is shown in Figure 1a. The figure shows the histogram of deviations of observed MP distance from the Earth,

R_{obs} from the Lin et al. (2010) model prediction, R_{mod}. The red line stands for the Gaussian fit and its parameters (Center, C and Full Width at Half Maximum, FWHM) are given at the figure top. We applied the same procedure to other models and the results are very similar ($C = 0.17$ and FWHM $= 1.32$ for Shue et al. (1997); $C = 0.12$ and FWHM $= 1.37$ for Petrinec and Russell (1996); $C = −0.09$ and FWHM $= 1.66$ for Jelínek et al. (2012); all values in R_E units). This result is surprising because the models use very different functional forms of the MP shape and different power exponents for the dependence of R_{mod} on upstream pressures. We select the Lin et al. (2010) model in our analysis because it exhibits the best agreement with observations.

As it can be seen from the figure, the Gaussian fit describes very well the shape of distributions with the exception of a small percentage of very large positive or negative $R_{obs} − R_{mod}$ values. The Gaussian core of the distribution is mostly a result of uncertainty of prediction of upstream parameters. Urbář et al. (2019) analyzed a relation between THEMIS observations in front of the BS and Wind measurements at L1 and they have shown that FWHM of the distribution of velocity ratios is as large as 0.05. The conversion of this value to the uncertainty of the subsolar MP prediction leads to FWHM of about 1.1 R_E. This value is a little lower than but comparable with those characterizing the uncertainties of model predictions.

For the reasons given above, our analysis concentrates on the large deviations from the model. Figure 1b shows the plot of $R_{obs} − R_{mod}$ as a function of R_{obs} for all dayside MP crossings. The gray dots stay for individual crossings and the colored bars stand for medians in 1 R_E distance bins. These medians are close to zero for distances between 8 and 12 R_E for all three subsets of crossings (subsolar–green, dawn–red, dusk–blue) but systematic positive deviations are observed at larger distances. This is especially true for our subsolar subset (crossings in the 30° cone around the X axis). It should be noted that similar plots for other MP models exhibit even larger deviations.

There can be several reasons for a bad prediction of the MP location: (a) influence of an upstream parameter not included in the model, (b) wrong propagation of upstream parameters and (c) effect of an IMF discontinuity. In order to check the first item, we have plotted R_{obs} as a function of different upstream parameters and found that the largest R_{obs} are connected with intervals of nearly radial IMF, in agreement with findings of Grimmich et al. (2023). Other conditions like a small dynamic pressure or small IMF strength are either included in the models or follow from properties of radial IMF intervals (Pi et al., 2014, 2017). The dependence of R_{obs} on the IMF cone angle is plotted in Figure 1c. The red bars show medians in distance bins and, despite the large spread of points, one can see a clear decreasing trend. It suggests that the addition of the cone angle to the parameters of the MP model can improve its precision (see also Dušík et al. (2010)), but this is out of the scope of the present study. However, if IMF points radially, the subsolar BS is almost parallel and the MP would be behind a strong foreshock and thus transient effects connected with foreshock fluctuations can be expected. For these reasons the next section describes several case studies that elucidate effects of the solar wind or IMF discontinuities as well as magnetosheath transients.

3. Magnetopause Location and Magnetosheath Transients

The first example uses observations of THEMIS B and C (THB and THC hereafter) on 2008-07-18 from 1320 to 1400 UT. THB located at (23.8, 4.7, −8.6) R_E serves as the upstream monitor whereas THC at (14.9, 3.7, −5.3) R_E was located close to the predicted BS location (Jeřáb et al., 2005) and finally, THD (8.4, 3.3, −3.1) R_E scans the MP on the magnetosphere side (no MP crossings were observed through the selected time interval). Note that we are using GSE coordinates in the paper. Figures 2a–2d (left part) show the magnetic field strength and three components, the dynamic pressure calculated from THB density and velocity measurements (d), and ion spectrogram. One can note the dynamic pressure below 0.8 nPa and almost radial IMF modulated by foreshock fluctuations caused by the high energy tail of the ion distribution visible in Figure 2c, but no notable IMF discontinuity is registered. Figures 2e–2h present the THC magnetic field, ion spectrogram, velocity components and dynamic pressure. The green line in the panel 2h shows half of the solar wind dynamic pressure because this level is usually considered for magnetosheath jet identification (Plaschke et al., 2017). The regions visited by THC are identified by color bars in the magnetic field panel (magnetosheath—-blue, magnetosphere—green, solar wind—red). Figure 2i shows the model distance of the BS (blue) and MP (green) along the direction toward the THC location together with the THC radial distance (black).

Consistently with the predicted MP location, THC is located in the magnetosheath until 1332 UT when it would cross the BS according to the model prediction (Figure 2i) but it enters the magnetosphere for about 8 min, then
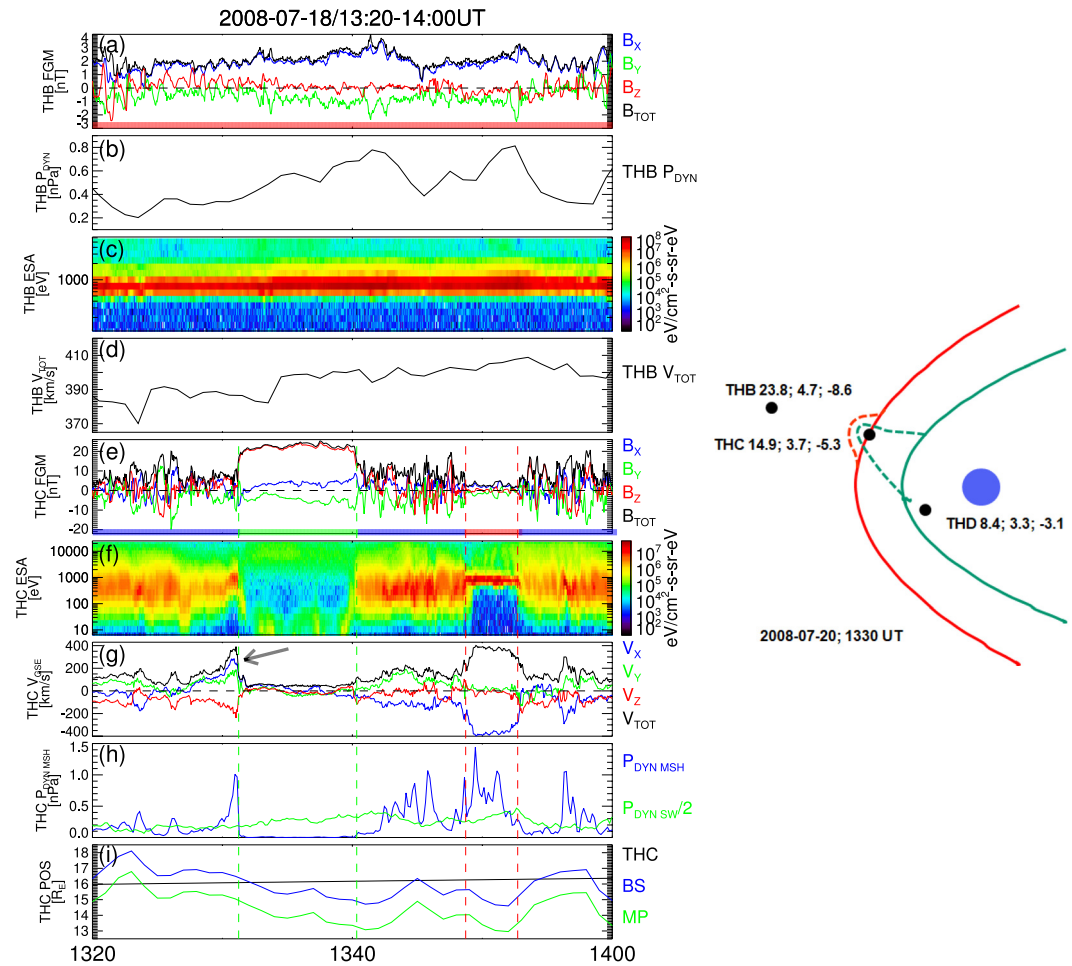
Figure 2. (left) Observations of THB and THC: (a) IMF magnitude and components; (b) solar wind dynamic pressure; (c) ion spectrogram; (d) solar wind velocity; (e) THC magnetic field; (f) THC ion spectrogram; (g) THC ion velocity and its components; (h) magnetosheath dynamic pressure and a half of the upstream dynamic pressure from panel (b); and (i) predicted distance of both BS and MP from the Earth along the direction coming through THC. Green and red vertical lines mark the MP and BS crossings, the black arrow indicates the observation of the sunward flow. (right) Sketch of approximate BS and MP locations and the shapes together with spacecraft locations (see text for the description). The visited regions are marked by color bars in the magnetic field panel (magnetosheath—-blue, magnetosphere—green, solar wind—red).

it returns to the magnetosheath, and around 1350 UT it undergoes two BS crossings. Times of these BS crossings are reasonably predicted by the model, on the other hand, the MP crossings are very far from the prediction (3 R_E for the second one). A sketch in the right part shows an approximate shape of the boundaries during the event. One can see the large but the short-time (and probably spatially limited) MP displacement, similar to that reported for interaction of the magnetosphere with HFA. However, no IMF discontinuity is observed upstream and the level of foreshock fluctuations is moderate. The only notable feature is a strong sunward flow in the magnetosheath just prior to the first MP crossing (black arrow in Figure 2g).

Figure 3 presents observations on 2008-08-20 around 2220 UT. Since none of the spacecraft was just upstream, Figures 3a and 3b use the ACE magnetic field and dynamic pressure propagated to the THC location by the two-step routine (Šafránková et al., 2002). We observe a very quiet nearly radial IMF without any discontinuity and about constant dynamic pressure below 1 nPa. THC was again close to the predicted BS location (Figure 3l) slightly dawnward from the subsolar point. This location is consistent with observations shown in the panels c–f that reveal several solar wind/foreshock intervals characterized by large negative values of the Vx velocity component (Figure 3e) and low IMF strength (Figure 3c). However, a clear entry to the magnetosphere distinguished by green dashed vertical lines can be identified between 2217 and 2224 UT. It suggests an outward MP expansion but THE located in the magnetosphere about 1 R_E inward the predicted MP position (Figure 3l, green
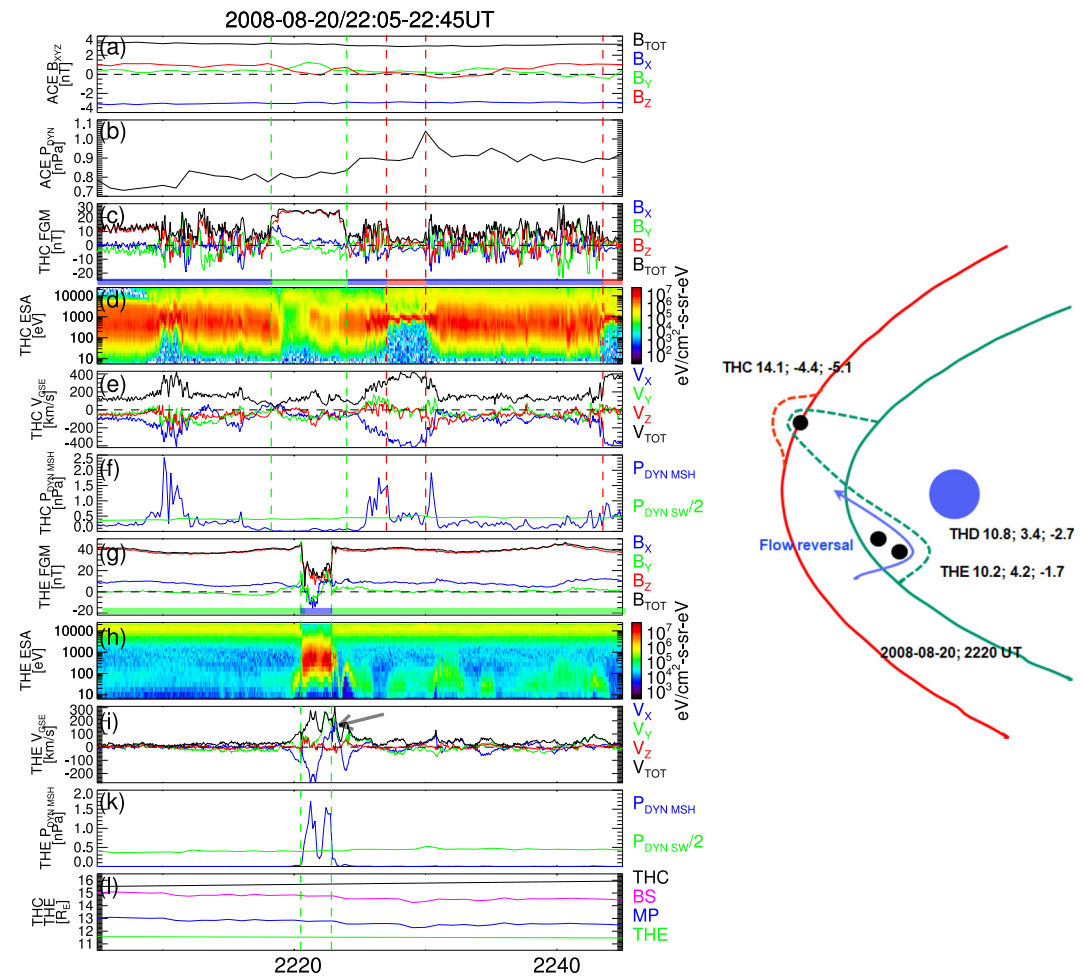
Figure 3. (left) Second example: (a, b) IMF components and solar wind dynamic pressure both propagated from ACE to the THC location; (c) THC magnetic field; (d) THC ion spectrogram; (e) THC proton velocity; (f) THC dynamic pressure; (g) THE magnetic field; (h) THE ion spectrogram; (i) THE proton velocity; (k) THE dynamic pressure; and (l) predicted distance of both BS and MP from the Earth along the direction coming through THC. Green and red vertical lines mark the MP and BS crossings, visited regions are marked by color bars in THC (c) and THE (f) magnetic field panels (magnetosheath——blue, magnetosphere—green, solar wind—red), the black arrow indicates the observation of the sunward flow. (right) Sketch of approximate BS and MP locations and shapes together with spacecraft positions (see text for the description).

line) enters the magnetosheath during this time interval (see color bars in Figure 3g), indicating a MP compression. As can be seen in the right-hand sketch, THC and THB observe simultaneous compression and expansion of the magnetosphere at two places separated by about 2 hr of the local time. This deformation is connected with the antisunward jet that reverses to the sunward direction just prior to the THC MP crossing. Even more clear reversal of the jet direction in the magnetosheath is observed by THE (Figure 3i, black arrow). THD that is closer to the model MP (not shown) observes similar but more pronounced features and the timing of THD—THE observations suggests that the MP distortion moves slowly dawnward.

Two examples discussed so far show the switch of the magnetosheath jet direction as an isolated phenomenon. However, Figure 4 presents observations of a series of such events, albeit only the first of them resulted in the MP deformation reaching the outbound spacecraft. The figure format follows Figure 3. The upstream parameters in Figures 4a and 4b propagated from ACE reveal again a nearly radial IMF and the dynamic pressure of about 0.8 nPa. Figures 4c–4f present the THC magnetic field, ion spectrogram, ion velocity components and dynamic pressure, respectively. THC was close to the BS and crossed it several times in course of the depicted interval (red vertical lines in Figures 4a–4f) but around 0020 UT it underwent a short excursion to the magnetosphere (green vertical lines), although it was about 4 R_E upstream from its predicted position (Figure 4l). The first MP
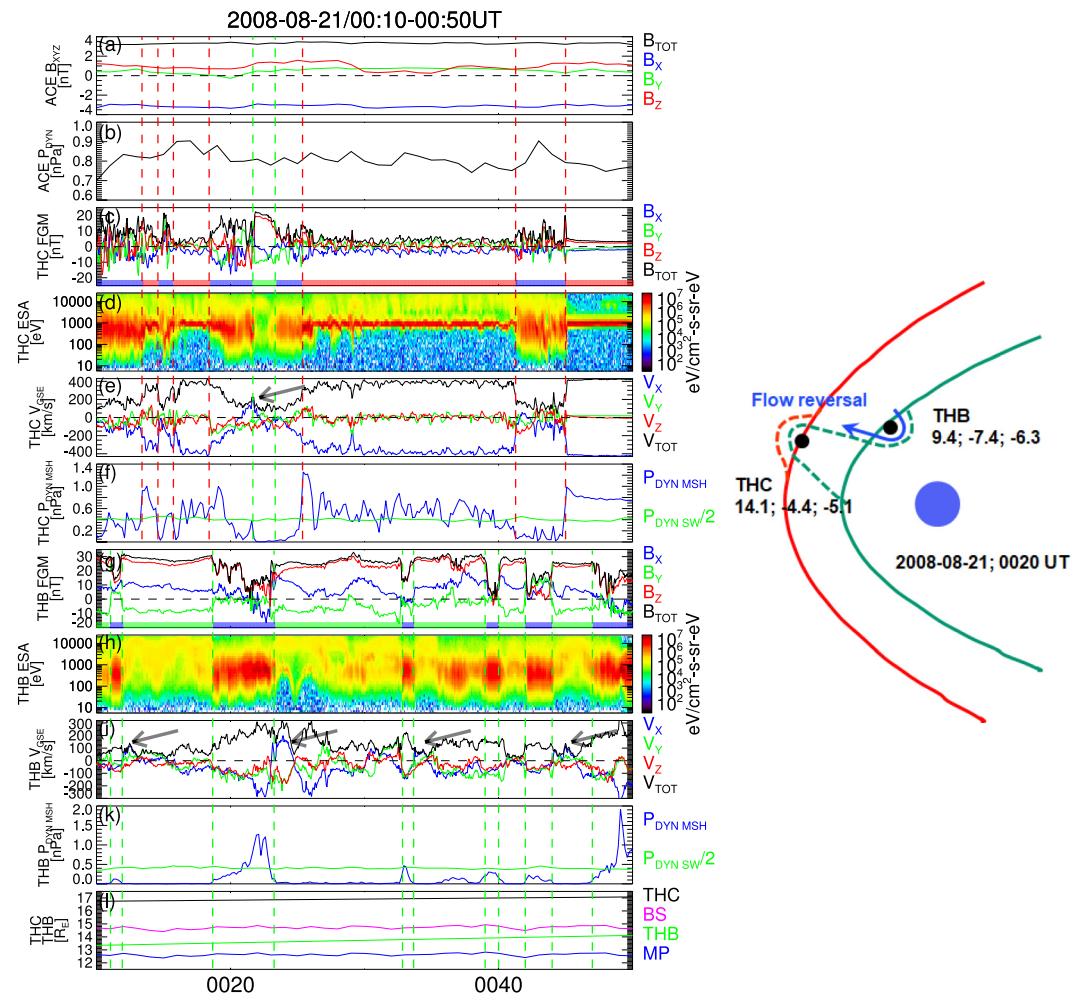
Figure 4. (left) Third example: The same format of the data as Figure 3, only THE observations are replaced by THB. (right) Sketch of approximate BS and MP locations and shapes together with spacecraft positions (see text for the description).

crossing is connected with a strong earthward jet that reverses its direction prior to the crossing. THB was in the magnetosheath during the THC magnetospheric interval, and it clearly shows the strong earthward jet followed by the sunward flow with the peak velocity of 200 km/s. These features resemble those shown in Figure 3 but between 0030 and 0050 UT, THB observed a series of MP crossings and nearly all of them are connected with the sunward flows (black arrows in Figure 4h). These flows are observed in the MP boundary layer and indicate a fast outward MP motion (Archer et al., 2014) but with an amplitude not sufficient to reach the THC location.

4. Discussion and Conclusion

The three examples shown in the previous section document observations of large outward displacements of the subsolar MP. These displacements are spatially limited and they are connected with the creation of a dip in the MP surface. The angular separation of the spacecraft observing simultaneously bump and dip was about 50° in the second and less than 30° in the third example. Such a localized MP deformation was already reported in a connection with HFAs. However, HFAs result from the interaction of the IMF tangential discontinuity with bow shock (Šafránková et al., 2012; Sibeck et al., 1999) but no such discontinuity was observed in our examples. All discussed events occur under a lower upstream pressure and nearly radial IMF. Such conditions are favorable for the creation of spontaneous HFAs (Chu et al., 2017) or magnetosheath jets (LaMoury et al., 2021), and some of them (and probably the most intensive ones) can be connected with the BS reformation as a natural part of the dynamical evolution of quasi-parallel collisionless shocks (Raptis et al., 2022). The enhanced pressure inside a

jet pushes the MP inward locally, creating a dip in its surface. The dip turns the jet toward the sunward direction (Shue et al., 2009). The sunward moving jet depletes a localized region in front of the MP (Archer et al., 2014), and it thus moves sunward.

This scenario prefers the creation of sunward jets leading to extreme MP displacements by mechanism described by Shue et al. (2009), as clear dips on the MP surface were documented in our second and third examples. We have also checked other possible mechanisms suggested for the sunward flow formation, like MP reconnection (Ng et al., 2021) or Kelvin-Helmholtz instability (Yan et al., 2020). Since the reconnection jets should move along the magnetic field, we have plotted the angle between the velocity and magnetic field (not shown). This angle is small in the solar wind and outer magnetosheath but it is in the range of $60 - -120°$ within the intervals of sunward flows and it rules out reconnection as a possible source of them. The Kelvin-Helmholtz instability is typical at the flanks because it requires a sufficient velocity shear across the MP and thus it cannot cause sunward jets in the subsolar region. On the other hand, series of less intensive sunward jets shown in our third example can result from the interaction of earthward jets with magnetosheath plasma as suggested by Plaschke et al. (2017).

Our scenario includes both the inward and outward MP displacements but the inward displacements are relatively modest ($1 - 2\,R_E$ from the model position) in all cases. It is consistent with the statistics in Figure 1b because the model statistically predicts the MP rather well if it is observed closer than $12\,R_E$ from the Earth. In contrast, the outward MP displacement can exceed $4\,R_E$ from the predicted location. Nevertheless, out of 50,000 dayside crossings only about 0.5% are farther than $2\,R_E$ from the predicted locations. However, the real occurrence rate of such events is probably several times higher, because our observations demonstrate that the MP deformations are localized in space and time and only a spacecraft that is, by a chance, at the appropriate local time and sufficiently far from the Earth can register them.

A hint of the real occurrence rate of extreme MP displacements could come from detailed studies of wave processes. For example, Katsavrias et al. (2021) report significant enhancements of Pi2 pulsation activity connected with the sunward flows in the magnetosheath. A first step in this direction is a case study of different wave emissions inside and in the vicinity of jets by Krämer et al. (2023) that contributes to understanding the microphysics of the jets with motivation to gain a knowledge about their evolution and formation.

Although our study is limited to the subsolar region, Figure 1b suggests that similar effects can be probably observed along the whole dayside MP. The median values of $R_{obs} - -R_{mod}$ indicate a weaker effect, but it should be taken into account that the THEMIS apogee was relatively low and the average MP position is much farther from the Earth at morning or afternoon local times and the real MP deformation magnitude thus cannot be recorded.

Last but not least, we should point out that, although preferable solar wind conditions for observations of extreme MP locations are a low cone angle and low dynamic pressure, the investigated effects are localized and transient and cannot be captured by empirical MP models. **These models are frequently used in studies of the magnetosheath jets, see for examples** Goncharov et al. (2020), Raptis et al. (2020), LaMoury et al. (2021), and Vuorinen et al. (2021)**, but our results show that their predictions should be applied with a special care in a highly disturbed magnetosheath.** On the other hand, the fact that our events were observed under a nearly radial magnetic field in a combination with the aforementioned THEMIS orbital limitation probably led Merka et al. (2003) to the suggestion of a bullet like MP shape under a radial IMF.

Data Availability Statement

THEMIS-ARTEMIS magnetic field and plasma data are public and are available at artemis.ssl.berkeley.edu or cdaweb.gsfc.nasa.gov/pub/data/themis; ACE and OMNI data can be accessed via cdaweb.gsfc.nasa.gov/cgi-bin/eval1.cgi using the particular time intervals of events for identification of the magnetic field and plasma data.

References

Angelopoulos, V. (2008). The THEMIS mission. *Space Science Reviews*, *141*(1–4), 5–34. https://doi.org/10.1007/s11214-008-9336-1

Archer, M. O., Turner, D. L., Eastwood, J. P., Horbury, T. S., & Schwartz, S. J. (2014). The role of pressure gradients in driving sunward magnetosheath flows and magnetopause motion. *Journal of Geophysical Research: Space Physics*, *119*(10), 8117–8125. https://doi.org/10.1002/2014JA020342

Auster, H. U., Glassmeier, K. H., Magnes, W., Aydogar, O., Baumjohann, W., Constantinescu, D., et al. (2008). The THEMIS fluxgate magnetometer. *Space Science Reviews*, *141*(1–4), 235–264. https://doi.org/10.1007/s11214-008-9365-9

Boardsen, S., Eastman, T., Sotirelis, T., & Green, J. (2000). An empirical model of the high-latitude magnetopause. *Journal of Geophysical Research*, *105*(A10), 23193–23219. https://doi.org/10.1029/1998JA000143

Chu, C., Zhang, H., Sibeck, D., Otto, A., Zong, Q., Omidi, N., et al. (2017). Themis satellite observations of hot flow anomalies at Earth's bow shock. *Annales Geophysicae*, *35*(3), 443–451. https://doi.org/10.5194/angeo-35-443-2017

Dušík, Š., Granko, G., Šafránková, J., Němeček, Z., & Jelínek, K. (2010). IMF cone angle control of the magnetopause location: Statistical study. *Geophysical Research Letters*, *37*(19), L19103. https://doi.org/10.1029/2010GL044965

Goncharov, O., Gunell, H., Hamrin, M., & Chong, S. (2020). Evolution of high-speed jets and plasmoids downstream of the quasi-perpendicular bow shock. *Journal of Geophysical Research: Space Physics*, *125*(6), e2019JA027667. https://doi.org/10.1029/2019JA027667

Grimmich, N., Plaschke, F., Archer, M. O., Heyner, D., Mieth, J. Z. D., Nakamura, R., & Sibeck, D. G. (2023). Study of extreme magnetopause distortions under varying solar wind conditions. *Journal of Geophysical Research: Space Physics*, *128*(8), e2023JA031603. https://doi.org/10.1029/2023JA031603

Gu, Y. X., Wang, Y., Wei, F. S., Feng, X. S., Song, X. J., Wang, B. Y., et al. (2023). Quasi-elastodynamic processes involved in the interaction between solar wind and magnetosphere. *The Astrophysical Journal*, *946*(2), 102. https://doi.org/10.3847/1538-4357/acbe9b

Jacobsen, K. S., Phan, T. D., Eastwood, J. P., Sibeck, D. G., Moen, J. I., Angelopoulos, V., et al. (2009). THEMIS observations of extreme magnetopause motion caused by a hot flow anomaly. *Journal of Geophysical Research*, *114*(A8), A08210. https://doi.org/10.1029/2008JA013873

Jelínek, K., Němeček, Z., & Šafránková, J. (2012). A new approach to magnetopause and bow shock modeling based on automated region identification. *Journal of Geophysical Research*, *117*(A5), A05208. https://doi.org/10.1029/2011JA017252

Jeřáb, M., Němeček, Z., Šafránková, J., Jelínek, K., & Měrka, J. (2005). Improved bow shock model with dependence on the IMF strength. *Planetary and Space Science*, *53*(1–3), 85–93. https://doi.org/10.1016/j.pss.2004.09.032

Katsavrias, C., Raptis, S., Daglis, I. A., Karlsson, T., Georgiou, M., & Balasis, G. (2021). On the generation of Pi2 pulsations due to plasma flow patterns around magnetosheath jets. *Geophysical Research Letters*, *48*(15), e2021GL093611. https://doi.org/10.1029/2021GL093611

Krämer, E., Hamrin, M., Gunell, H., Karlsson, T., Steinvall, K., Goncharov, O., & Andre, M. (2023). Waves in magnetosheath jets-classification and the search for generation mechanisms using mms burst mode data. *Journal of Geophysical Research: Space Physics*, *128*(7), e2023JA031621. https://doi.org/10.1029/2023JA031621

LaMoury, A. T., Hietala, H., Plaschke, F., Vuorinen, L., & Eastwood, J. P. (2021). Solar wind control of magnetosheath jet formation and propagation to the magnetopause. *Journal of Geophysical Research: Space Physics*, *126*(9), e2021JA029592. https://doi.org/10.1029/2021JA029592

Lin, R. L., Zhang, X. X., Liu, S. Q., Wang, Y. L., & Gong, J. C. (2010). A three-dimensional asymmetric magnetopause model. *Journal of Geophysical Research*, *115*(A4), A04207. https://doi.org/10.1029/2009JA014235

Liu, Z. Q., Lu, J. Y., Wang, C., Kabin, K., Zhao, J. S., Wang, M., et al. (2015). A three-dimensional high Mach number asymmetric magnetopause model from global MHD simulation. *Journal of Geophysical Research: Space Physics*, *120*(7), 5645–5666. https://doi.org/10.1002/2014JA020961

Machková, A., Němec, F., Němeček, Z., & Šafránková, J. (2019). On the influence of the Earth's magnetic dipole eccentricity and magnetospheric ring current on the magnetopause location. *Journal of Geophysical Research: Space Physics*, *124*(2), 905–914. https://doi.org/10.1029/2018JA026070

McFadden, J. P., Carlson, C. W., Larson, D., Ludlam, M., Abiad, R., Elliott, B., et al. (2008). The THEMIS ESA plasma instrument and in-flight calibration. *Space Science Reviews*, *141*(1–4), 277–302. https://doi.org/10.1007/s11214-008-9440-2

Merka, J., Szabo, A., Šafránková, J., & Němeček, Z. (2003). Earth's bow shock and magnetopause in the case of a field-aligned upstream flow: Observation and model comparison. *Journal of Geophysical Research*, *108*(A7), 1269. https://doi.org/10.1029/2002JA009697

Ng, J., Chen, L.-J., & Omelchenko, Y. A. (2021). Bursty magnetic reconnection at the Earth's magnetopause triggered by high-speed jets. *Physics of Plasmas*, *28*(9). https://doi.org/10.1063/5.0054394

Nguyen, G., Aunai, N., Michotte de Welle, B., Jeandet, A., Lavraud, B., & Fontaine, D. (2022). Massive multi-mission statistical study and analytical modeling of the Earth's magnetopause: 2. Shape and location. *Journal of Geophysical Research: Space Physics*, *127*(1), e2021JA029774. https://doi.org/10.1029/2021JA029774

Petrinec, S. M., & Russell, C. T. (1996). Near-Earth magnetotail shape and size as determined from the magnetopause flaring angle. *Journal of Geophysical Research*, *101*(A1), 137–152. https://doi.org/10.1029/95JA02834

Pi, G., Shue, J.-H., Chao, J.-K., Němeček, Z., Šafránková, J., & Lin, C.-H. (2014). A reexamination of long-duration radial IMF events. *Journal of Geophysical Research: Space Physics*, *119*(9), 7005–7011. https://doi.org/10.1002/2014JA019993

Pi, G., Shue, J.-H., Grygorov, K., Li, H.-M., Němeček, Z., Šafránková, J., et al. (2017). Evolution of the magnetic field structure outside the magnetopause under radial IMF conditions. *Journal of Geophysical Research: Space Physics*, *122*(4), 4051–4063. https://doi.org/10.1002/2015JA021809

Plaschke, F., Karlsson, T., Hietala, H., Archer, M., Voeroes, Z., Nakamura, R., et al. (2017). Magnetosheath high-speed jets: Internal structure and interaction with ambient plasma. *Journal of Geophysical Research: Space Physics*, *122*(10), 10157–10175. https://doi.org/10.1002/2017JA024471

Raptis, S., Karlsson, T., Plaschke, F., Kullen, A., & Lindqvist, P.-A. (2020). Classifying magnetosheath jets using mms: Statistical properties. *Journal of Geophysical Research: Space Physics*, *125*(11), e2019JA027754. https://doi.org/10.1029/2019JA027754

Raptis, S., Karlsson, T., Vaivads, A., Pollock, C., Plaschke, F., Johlander, A., et al. (2022). Downstream high-speed plasma jet generation as a direct consequence of shock reformation. *Nature Communications*, *13*(1), 986. https://doi.org/10.1038/s41467-022-28664-3

Šafránková, J., Dušík, Š., & Němeček, Z. (2005). The shape and location of the high-latitude magnetopause. *Advances in Space Research*, *36*(10), 1934–1939. https://doi.org/10.1016/j.asr.2004.05.009

Šafránková, J., Goncharov, O., Němeček, Z., Přech, L., & Sibeck, D. G. (2012). Asymmetric magnetosphere deformation driven by hot flow anomaly(ies). *Geophysical Research Letters*, *39*(15), L15107. https://doi.org/10.1029/2012GL052636

Šafránková, J., Němeček, Z., Dušík, Š., Přech, L., Sibeck, D., & Borodkova, N. (2002). The magnetopause shape and location: A comparison of the Interball and Geotail observations with models. *Annales Geophysicae*, *20*(3), 301–309. https://doi.org/10.5194/angeo-20-301-2002

Samsonov, A. A., Bogdanova, Y. V., Branduardi-Raymont, G., Šafránková, J., Němeček, Z., & Park, J.-S. (2019). Long-term variations in solar wind parameters, magnetopause location, and geomagnetic activity over the last five solar cycles. *Journal of Geophysical Research: Space Physics*, *124*(6), 4049–4063. https://doi.org/10.1029/2018JA026355

Shue, J. H., Chao, J. K., Fu, H. C., Russell, C. T., Song, P., Khurana, K. K., & Singer, H. J. (1997). A new functional form to study the solar wind control of the magnetopause size and shape. *Journal of Geophysical Research*, *102*(A5), 9497–9512. https://doi.org/10.1029/97JA00196

Shue, J. H., Chao, J. K., Song, P., McFadden, J. P., Suvorova, A., Angelopoulos, V., et al. (2009). Anomalous magnetosheath flows and distorted subsolar magnetopause for radial interplanetary magnetic fields. *Geophysical Research Letters*, *36*(18), L18112. https://doi.org/10.1029/2009GL039842

Sibeck, D., Borodkova, N., Schwartz, S., Owen, C., Kessel, R., Kokubun, S., et al. (1999). Comprehensive study of the magnetospheric response to a hot flow anomaly. *Journal of Geophysical Research*, *104*(A3), 4577–4593. https://doi.org/10.1029/1998JA900021

Staples, F. A., Rae, I. J., Forsyth, C., Smith, A. R. A., Murphy, K. R., Raymer, K. M., et al. (2020). Do statistical models capture the dynamics of the magnetopause during sudden magnetospheric compressions? *Journal of Geophysical Research: Space Physics*, *125*(4), e2019JA027289. https://doi.org/10.1029/2019JA027289

Suvorova, A., Dmitriev, A., Chao, J., Thomsen, M., & Yang, Y. (2005). Necessary conditions for geosynchronous magnetopause crossings. *Journal of Geophysical Research*, *110*(A1), A01206. https://doi.org/10.1029/2003JA010079

Urbář, J., Němeček, Z., Šafránková, J., & Přech, L. (2019). Solar wind proton deceleration in front of the terrestrial bow shock. *Journal of Geophysical Research: Space Physics*, *124*(8), 6553–6565. https://doi.org/10.1029/2019JA026734

Vuorinen, L., Hietala, H., Plaschke, F., & LaMoury, A. T. (2021). Magnetic field in magnetosheath jets: A statistical study of B_z near the magnetopause. *Journal of Geophysical Research: Space Physics*, *126*(9), e2021JA029188. https://doi.org/10.1029/2021JA029188

Wang, Y., Sibeck, D. G., Merka, J., Boardsen, S. A., Karimabadi, H., Sipes, T. B., et al. (2013). A new three-dimensional magnetopause model with a support vector regression machine and a large database of multiple spacecraft observations. *Journal of Geophysical Research: Space Physics*, *118*(5), 2173–2184. https://doi.org/10.1002/jgra.50226

Xu, Q., Tang, B., Sun, T., Li, W., Zhang, X., Wei, F., et al. (2022). Modeling of the subsolar magnetopause motion under interplanetary magnetic field southward turning. *Space Weather: The International Journal of Research and Applications*, *20*(12). https://doi.org/10.1029/2022SW003250

Yan, G. Q., Parks, G. K., Cai, C. L., Chen, T., McFadden, J. P., & Ren, Y. (2020). Plasma transport into the duskside magnetopause caused by Kelvin-Helmholtz vortices in response to the northward turning of the interplanetary magnetic field observed by THEMIS. *Annales Geophysicae*, *38*(1), 263–273. https://doi.org/10.5194/angeo-38-263-2020